A Thiophene-Based Anchoring Ligand and Its Heteroleptic Ru(II)-Complex for Efficient Thin-Film Dye-Sensitized Solar Cells

Amaresh Mishra, Nuttapol Pootrakulchote, Mingkui Wang, Soo-Jin Moon, Shaik M. Zakeeruddin,* Michael Grätzel,* and Peter Bäuerle**

A novel heteroleptic Ru^{II} complex (BTC-2) employing 5,5′-(2,2′-bipyridine-4,4′-diyl)-*bis*(thiophene-2-carboxylic acid) (BTC) as the anchoring group and 4,4′- dinonyl-2,2′-bipiridyl and two thiocyanates as ligands is prepared. The photovoltaic performance and device stability achieved with this sensitizer are compared to those of the Z-907 dye, which lacks the thiophene moieties. For thin mesoporous TiO_2 films, the devices with BTC-2 achieve higher power conversion efficiencies than those of Z-907 but with a double-layer thicker film the device performance is similar. Using a volatile electrolyte and a double layer 7 + 5 μm mesoporous TiO_2 film, BTC-2 achieves a solar-to-electricity conversion efficiency of 9.1% under standard global AM 1.5 sunlight. Using this sensitizer in combination with a low volatile electrolyte, a photovoltaic efficiency of 8.3% is obtained under standard global AM 1.5 sunlight. These devices show excellent stability when subjected to light soaking at 60 °C for 1000 h. Electrochemical impedance spectroscopy and transient photovoltage decay measurements are performed to help understand the changes in the photovoltaic parameters during the aging process. In solid state dye-sensitized solar cells (DSSCs) using an organic hole-transporting material (spiro-MeOTAD, 2,2′,7,7′-tetrakis-(*N*,*N*-di-*p*-methoxyphenylamine)-9,9′-spirobifluorene), the BTC-2 sensitizer exhibits an overall power conversion efficiency of 3.6% under AM 1.5 solar (100 mW cm^{-2}) irradiation.

1. Introduction

Since the first report of a mesoscopic TiO_2-based dye-sensitized solar cell (DSSC) by O'Regan and Grätzel in 1991, this solar cell architecture has emerged as a promising candidate for practical photovoltaic applications by virtue of their low manufacturing costs and good conversion efficiencies.[1,2] Numerous sensitizers have been prepared and their performance has been tested. DSSCs with power conversion efficiencies over 10% under AM 1.5 irradiation were initially demonstrated using prototype *cis*-di(thiocyanato)-*bis*[2,2′-bipyridyl-4,4′-dicarboxylic acid] ruthenium(II) **N3**, its *bis*-tetrabutylammonium (TBA) salt counterpart **N719**, or the black dye [tri(thiocyanato)-(4,4′,4″-[2,2′:6′,2″-terpyridine] tricarboxylic acid] ruthenium(II) as sensitizers in combination with thicker titania films (>12–15 μm) and volatile electrolytes.[2] In DSSCs, the sensitizer is one of the critical components because it absorbs sunlight and induces intramolecular charge transfer from the ancillary to the anchoring ligand with subsequent electron injection to the TiO_2 via the carboxylic acid groups. Then, the electron is transported to and collected at an electrode. Subsequent hole transfer from the oxidized dye to I^-/I_3^- takes place, where the hole is transported to and collected at the counter electrode.[1] For an efficient DSSC, optimization of the short-circuit photocurrent (J_{SC}) and open-circuit potential (V_{OC}) of the cell is essential. Generally, V_{OC} is the difference between the quasi-Fermi level of the electrons under illumination in the TiO_2 and the redox potential of I^-/I_3^-. On the other hand, J_{SC} is related to the interaction between TiO_2 and the sensitizer, as well as the spectral response and molar extinction coefficient of the sensitizer.

To enhance the power conversion efficiencies of DSSCs, it is imperative to design novel sensitizers that exhibit an enhanced molar absorptivity in combination with a red-shift of the metal-to-ligand charge transfer (MLCT) transitions. Extension of the π-conjugation of the ancillary ligand and/or the anchoring ligand was found to improve the spectral response of corresponding ruthenium sensitizers.[3] Thus, efforts were recently made by incorporating thiophene derivatives into the ancillary bipyridine ligand in order to increase the molar extinction coefficient of the ruthenium dyes and to enhance their light-harvesting capacity as well as the spectral response.[4] With highly absorbing sensitizers it is possible to use thinner TiO_2

Dr. A. Mishra, Prof. P. Bäuerle
Institute of Organic Chemistry II and Advanced Materials
University of Ulm
Albert-Einstein-Allee 11, D-89081 Ulm, Germany
E-mail: amaresh.mishra@uni-ulm.de; peter.baeuerle@uni-ulm.de
N. Pootrakulchote, Dr. M. Wang, S.-J. Moon, Dr. S. M. Zakeeruddin, Prof. M. Grätzel
Laboratory for Photonics and Interfaces
Institute of Chemical Sciences and Engineering
School of Basic Sciences
Swiss Federal Institute of Technology
CH-1015, Switzerland
E-mail: shaik.zakeer@epfl.ch; michael.graetzel@epfl.ch

DOI: 10.1002/adfm.201001863

films to reduce recombination losses in order to generate high photocurrents.

We recently reported a novel anchoring ligand and its homoleptic ruthenium complex **BTC-1** composed of thiophene as an extended π-conjugated system in which the carboxylic acid groups are attached to the thiophene units.[5] This new strategy allowed us to obtain a red-shift of the MLCT absorption band together with an increased molar extinction coefficient of the sensitizer. Here, we present a novel amphiphilic heteroleptic Ru^{II} complex, referred to as **BTC-2**, in which the π-conjugation of the anchoring ligand is extended by incorporating thiophene units between the bipyridine and carboxylate groups. 4,4′-Dinonyl-2,2′-bipyridine is used as ancillary ligand. The advantage of amphiphilic sensitizer is to have a hydrophobic, compact monolayer on top of TiO_2 film such that there will be no water-induced dye desorption from the TiO_2 surface. This is the first time that an amphiphilic dye incorporating thiophene units in the anchoring ligand is presented. **BTC-2** has a higher molar absorption coefficient compared to standard counterpart **Z-907**, and its power-conversion efficiency (about 6%) is higher than that of **Z-907** in 3-μm thin TiO_2 films under the same cell fabrication and measurement conditions. This also corroborates well with the increased molar absorptivity and enhanced spectral response of the dye in the red wavelength region.

2. Results and Discussion

2.1. Synthesis

The new **BTC-2** sensitizer, in which the anchoring carboxylic acid group is attached to a thiophene moiety, was prepared according to **Scheme 1**. The synthesis of acid **1** was recently reported.[5] The heteroleptic amphiphilic complex **BTC-2** was prepared in a typical one-pot procedure starting from reaction of 4,4′-dinonyl-2,2′-bipyridine and di-μ-chloro(p-cymene) ruthenium(II) dimer in dimethylformamide (DMF) followed by reaction with ligand **1** and ammonium thiocyanate. The crude complex was dissolved in basic methanol solution and purified on a Sephadex LH-20 column using methanol as eluent. The structures were verified by ^{1}H NMR, ^{13}C NMR, and elemental analysis.

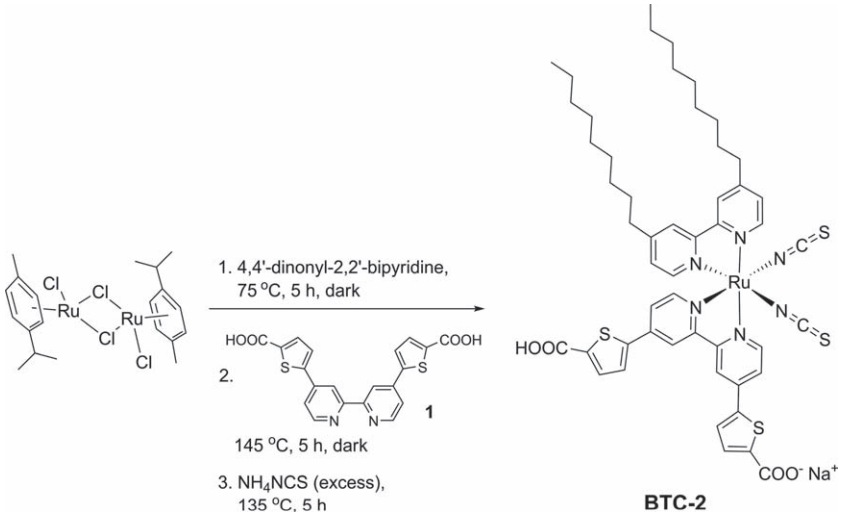

Scheme 1. Synthesis of the amphiphilic sensitizer **BTC-2**.

Table 1. Optical and electrochemical data of **BTC-2** and **Z-907** measured in DMF (HOMO/LUMO vs $Fc/Fc^+_{vac} = -5.1$ eV).

Dye	λ_{abs} [nm] (ε [L mol^{-1} cm^{-1}])	λ_{em} [nm]	E_{ox} [V]	E_{red} [V]	HOMO [eV]	LUMO [eV]	ΔE [eV]
BTC-2	548 (16 000)	805	0.20	−1.90	−5.22	−3.30	1.92
	422 (16 200)						
	341 (33 700)						
	299 (57 500)						
Z-907	526 (12 200)	760	0.26	−2.10	−5.28	−3.11	2.17
	370 (12 300)						
	298 (50 700)						

2.2. Steady-State Spectroscopy

The absorption and emission maxima of **BTC-2** measured in DMF solution are summarized in **Table 1** and compared to prototype complex **Z-907**. The absorption and normalized emission spectra are displayed in **Figure 1**. Complex **BTC-2** showed broad absorption bands in the 300 to 750 nm region. The two high-energy bands at 299 and 341 nm arise due to intraligand π–π* transitions. The lower energy part of the absorption spectrum of the complex is dominated by MLCT transitions with maxima at 422 and 548 nm. A red-shift of about 28 nm was observed for the lowest energy MLCT band of **BTC-2** compared to the standard **Z-907** sensitizer because of the extension of π-conjugation in the anchoring ligand and an increased highest occupied molecular orbital (HOMO) energy level. The low energy MLCT absorption band at 548 nm of the **BTC-2** dye has a molar extinction coefficient of 1.6×10^4 L mol^{-1} cm^{-1}, which is higher than the corresponding value for **Z-907** (1.2×10^4 L mol^{-1} cm^{-1}). Importantly, an increase of about 30% of the molar extinction coefficient was observed for the longest wavelength MLCT band as a consequence of the insertion of thiophene units to the ligand compared to **Z-907** sensitizer. The emission data of the dyes were obtained in an air-equilibrated DMF solution at 298 K by exciting at the respective low energy MLCT absorption band, showing a weak emission maximum at 805 nm for **BTC-2** and at 760 nm for **Z-907**.

2.3. Electrochemical Studies

Figure 2 shows typical cyclic voltammograms of **BTC-2** and **Z-907** in a DMF solution containing 0.1 M $TBAPF_6$ as supporting

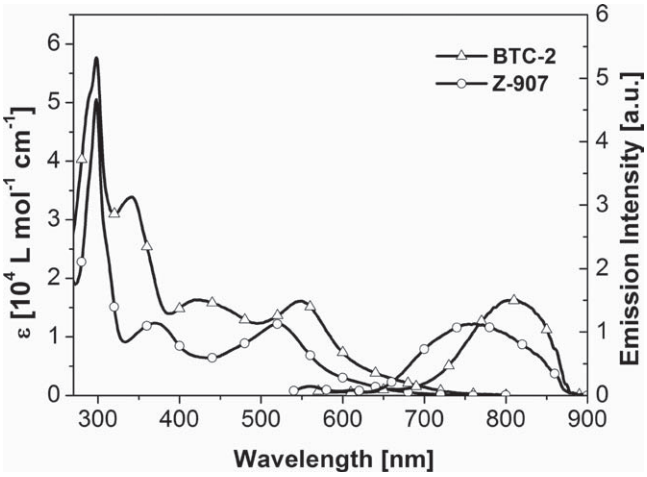

Figure 1. Absorption and emission spectra of **BTC-2** (triangles) and **Z-907** (circles) in DMF.

electrolyte. When the potential is scanned between –0.2 and 1.0 V, chemically reversible redox waves with formal potentials at 0.20 and 0.26 V (vs ferrocene/ferrocenium (Fc^+/Fc)) were observed, which can be attributed to the one electron oxidation of ruthenium center in both dyes. Compared to the standard **Z-907** dye, the metal center oxidation of **BTC-2** is cathodically shifted by 60 mV indicating the electron-rich character of the new ligand as a result of the insertion of thiophene units. A reversible reduction wave at –1.90 V (vs Fc^+/Fc) can be assigned to a one electron reduction of the anchoring ligand. The cathodic potential of **BTC-2** is 200 mV more positive than that of **Z-907**. HOMO and lowest unoccupied molecular orbital (LUMO) energy levels of **BTC-2** and **Z-907** were determined from the onset of the first oxidation and reduction potential and are presented in Table 1.

Furthermore, for a highly efficient sensitizer in DSSCs, the LUMO energy level should be compatible with the conduction band edge energy of the TiO_2 photoanode (–4.0 eV vs vacuum) and its HOMO should be sufficiently low in energy to accept electrons from the I^-/I_3^--based redox electrolyte (–4.83 eV vs vacuum). The HOMO level of **BTC-2** was determined to –5.22 eV and the LUMO level was –3.30 eV. Overall, the HOMO–LUMO band gap of **BTC-2** (E_g = 1.92 eV) is approximately 250 meV smaller compared to **Z-907** (E_g = 2.17 eV), which is also reflected in the red-shift of the absorption spectrum. It was found that the HOMO energy levels of **BTC-2** match well with the redox potential of I^-/I_3^- allowing regeneration of the dye cation. The LUMO level of the dye is much more negative than the conduction-band edge of TiO_2, thus providing a thermodynamic driving force for efficient electron injection. Therefore, the red-shifted absorption and higher molar extinction coefficient of **BTC-2** together with the well-matched energy levels should lead to a better conversion efficiency than the **Z-907** sensitizer.

To further confirm the electron distribution of the HOMO and LUMO, we optimized the geometry of the **BTC-2** sensitizer using a semiempirical calculation (ZINDO/1) and the results are displayed in **Figure 3**. The electron density in the HOMO is uniformly distributed over the thiocyanate (NCS) groups and the Ru^{II} center.[6] However, the electron density in the LUMO is mainly localized at the anchoring ligand, through which electron injection into the TiO_2 conduction band occurs.

2.4. Photovoltaic Performance

The photovoltaic performance of the sensitizers, i.e., the incident photon-to-current conversion efficiency (IPCE) and the photocurrent–voltage (*J*–*V*) curve, was assessed in test devices using standard mesoporous 7+5 μm thick TiO_2 films and a volatile acetonitrile-based electrolyte (**Figure 4**). Using 4-guanidino butyric acid (GBA) as a co-adsorbent the **BTC-2**-sensitized cell provided a short-circuit current density (J_{SC}) of 16.1 mA cm^{-2}, a open circuit voltage (V_{OC}) of 0.75 V, and a fill factor (*FF*) of 0.74, yielding an overall power conversion efficiency (η) of 9.1% under standard global AM 1.5 sunlight. The corresponding IPCE spectrum showed a plateau of over 80% from 455 to 620 nm, with the maximum of 85% at 550 nm. The J_{SC} agrees with the value calculated from the overlap integral of the IPCE spectrum with standard AM 1.5G solar emission spectrum showing that the spectral mismatch is less than 2%.

To demonstrate the potential of the **BTC-2** compared to the prototype dye, **Z-907**, which lacks the thiophene moieties in the anchoring groups, devices were prepared under identical conditions using the Z946 electrolyte with two mesoporous TiO_2 films of different thickness. The photovoltaic parameters of these devices are shown in **Figure 5** and the data are summarized in **Table 2**. It is evident that the J_{SC} values obtained with a 3-μm-thin TiO_2 film sensitized with the **BTC-2** dye are 18% higher than those of the corresponding devices prepared with **Z-907** dye. As the TiO_2 film thickness increases from 3 μm to 5 μm,

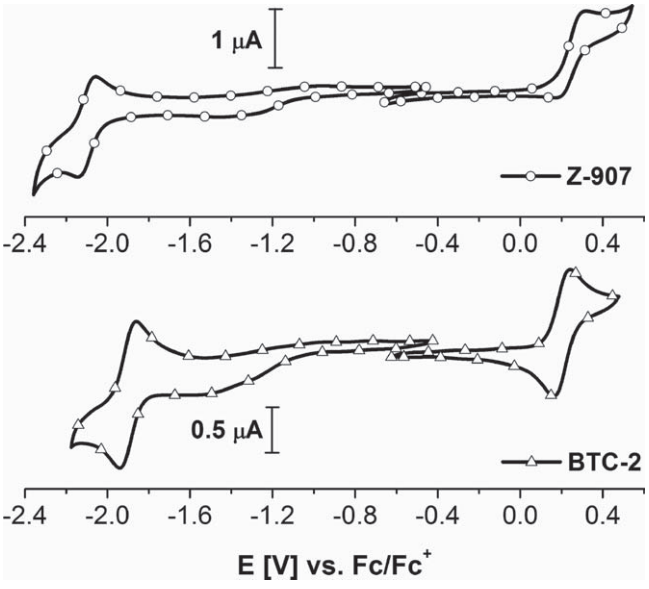

Figure 2. Cyclic voltammograms of **BTC-2** (triangles) and **Z-907** (circles) (1×10^{-3} mol L^{-1} in DMF). Tetrabutylammonium hexafluorophosphate ($TBAPF_6$; 0.1 M in DMF) is used as supporting electrolyte. All scan rates were 100 mV s^{-1}. The potentials were internally referenced to the ferrocene/ferrocenium (Fc^+/Fc) couple.

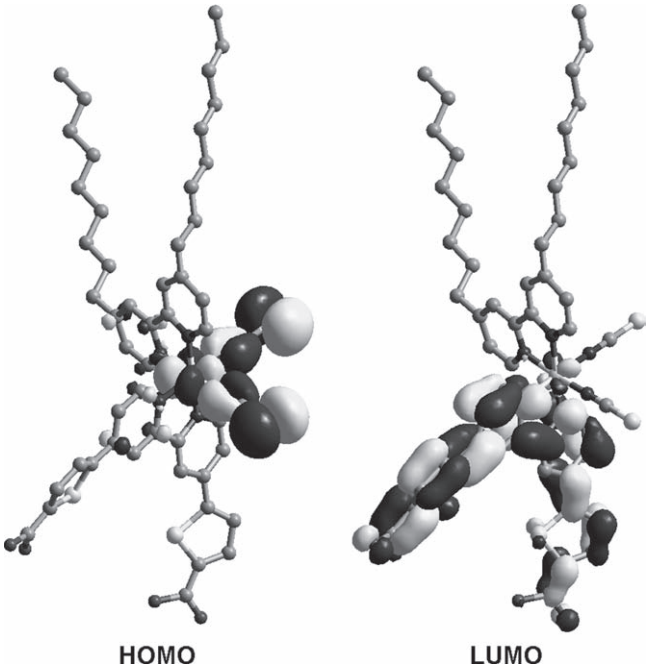

Figure 3. Graphical representation of the frontier orbitals (ZINDO/1 calculation) of **BTC-2** (hydrogens are omitted for clarity).

the J_{SC} values of devices using **BTC-2** are approximately 10% higher than those of the corresponding **Z-907** dye. With a double layer film (7 + 5 μm) a beneficial influence of the high molar extinction coefficient of sensitizer **BTC-2** over **Z-907** on the short circuit photocurrents was not observed because it was nullified by the presence of reflecting particles in the double layer structure TiO_2 film and practically the same values were obtained.

The long-term stability of a device is a crucial parameter for its practical application in photovoltaics. To demonstrate the potential of the **BTC-2** dye, devices based on **BTC-2** were optimized by using a double-layered TiO_2 film (7+5 μm) sensitized with **BTC-2** and GBA as a co-adsorbent, in conjunction with a low-volatile electrolyte based on 3-methoxypropionitrile as a solvent. The device B provided a J_{SC} of 15.1 mA cm^{-2}, a V_{OC} of 0.74 V, and a *FF* of 0.74, yielding an overall efficiency, η, of 8.3% under standard global AM 1.5 sunlight. In order to explore the stability of device B, the cell covered with a 50-μm-thick polyester film, which acted as a UV cut-off filter for the accelerated test, was illuminated with visible light (1 sun; 100 mW cm^{-2}) at 60 °C. After 1 000 h of light soaking and thermal stress, the photovoltaic parameters J_{SC}, V_{OC}, and *FF* of the cell were slightly changed to 15.0 mA cm^{-2}, 0.71 V, and 0.74, respectively, retaining 96% of its initial η value (**Figure 6**).

In order to understand the changes in the photovoltaic parameters during the ageing process, impedance spectral analysis was carried out with fresh and aged devices. Impedance analysis was likewise utilized to monitor the photovoltaic parameter changes in various devices.[4l,7–10] **Figure 7**a presents the effect of the applied voltage (U) on the electron transport resistance R_t under dark conditions for various devices. The electron transfer resistance depends on the density of electrons (n_{cb}) in the conduction band (CB) and the mobility (μ_e, the free

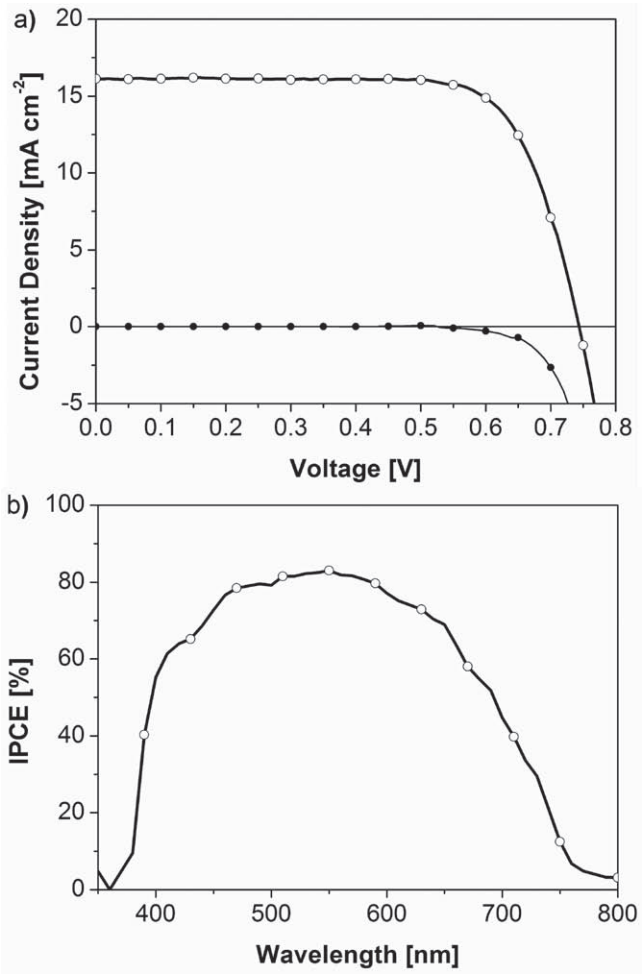

Figure 4. a) Photocurrent density–voltage (*J–V*) characteristics of a device using **BTC-2** as sensitizer and GBA as a co-adsorbent (open circles) under AM 1.5G illumination (100 mW cm^{-2}). Dark current is shown as filled circles. b) IPCE spectrum of the same device. Electrolyte composition (Z984): 1,3-dimethylimidazolium iodide = 0.6 M, iodine = 0.03 M, *tert*-butylpyridine = 0.5 M, LiI = 0.05 M, guanidinium thiocyanate = 0.1 M, in an acetonitrile:valeronitrile mixture (85:15 v/v). TiO_2 film contains a double layer with film thickness 7 + 5 μm.

electrons diffusion coefficient according to the Einstein relation on diffusion of charged particles).[7,11] The R_t data from the fresh device B are shifted downward (+30 mV) from those of the fresh device A, which is caused by a shift in the conduction band edge of TiO_2, E_{cb}, towards higher values in fresh device B.[6] Without considering the change in electron mobility (μ_e), in case of the fresh device B, an upward shift of E_{cb} by approximately 88 mV with respect to the Fermi level of the redox couple was observed compared to that of the aged sample using the same electrolyte. Figure 7b presents the capacitance (C_μ) versus R_t. Note that an identical resistance means that if the difference in charge mobility is ignored, an equal number of electrons, i.e., the same distance between Fermi level (E_F) and E_{cb}, was assumed.

Device B, and in particular the aged device B, showed an augmented chemical capacitance, indicating that more trap states were produced during light soaking and thermal stress, inferring

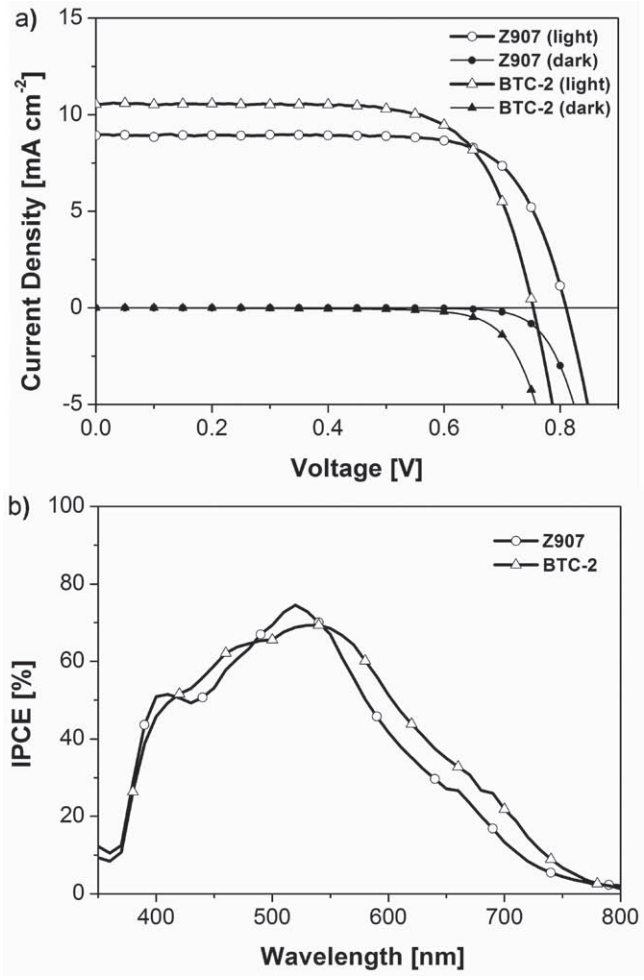

Figure 5. *J–V* characteristic of a) a device using **BTC-2** and **Z-907** sensitizers and GBA as a co-adsorbent under AM 1.5G illumination (100 mW cm^{-2}). b) IPCE spectra of the same device. Electrolyte composition (Z946): 1,3-dimethylimidazolium iodide = 1.0 M, iodine = 0.15 M, *N*-butyl benzimidazole = 0.5 M, guanidinium thiocyanate = 0.1 M, in 3-methoxy propionitrile. TiO_2 film contains a transparent layer of 3 μm thickness.

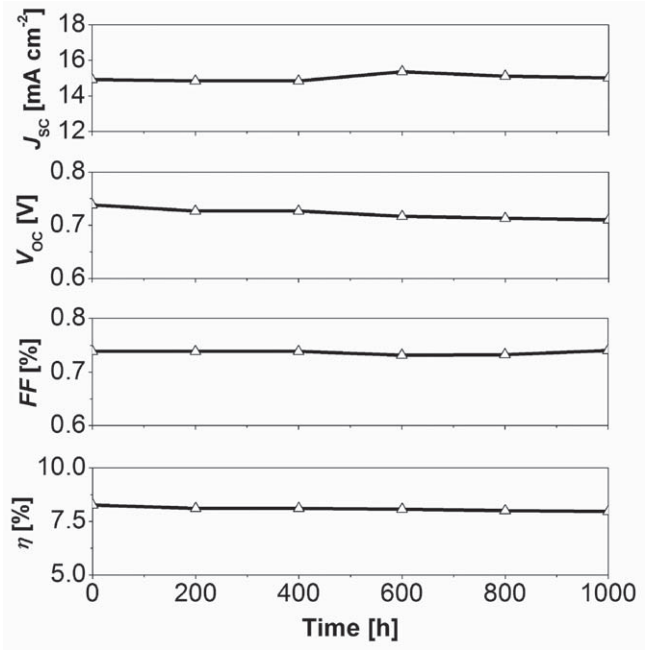

Figure 6. Evolution of the photovoltaic parameters (J_{SC}, V_{OC}, *FF*, and η) for the device based on a 7+5-μm-thick TiO_2 double layer film sensitized with **BTC-2** in the presence of GBA (1:1 molar ratio) as the co-adsorbent and low volatility liquid electrolyte.

that μ_e in the aged device could have an influence on the electron transfer resistance. Figure 7c presents the overall recombination resistance (R_{ct}) for the charge transfer at the TiO_2/eletrolyte interface with R_t.[12] The fresh device B has largest R_{ct} compared to the aged device at an identical R_t. This result can be attributed to the formation of a more compact monolayer on the film's surface when GBA is cografted compared to that formed in the presence of sensitizer alone. After light soaking, the R_{ct} values of the aged device became similar to those of the fresh device A. All devices have a larger value of R_{ct} than R_t, indicating an effective collection of photogenerated charge carriers in the dye-sensitized heterojunction. A slightly decreased apparent electron diffusion coefficient ($D_n = d/R_tC_\mu$, where d is the film thickness) in the devices B was observed and is illustrated in Figure 7d. This indicates that the GBA has a small influence on the electron transport in the TiO_2 nanoparticles, which might be due to the creation of surface states. For the aged sample, a large decrease in the apparent electron diffusion coefficient was observed under identical R_t, clarifying the influence of the light soaking and thermal stress on the dye-sensitized TiO_2 nanocrystalline film.

Table 2. Photovoltaic parameters of devices with TiO_2 films of various thicknesses. Device A: without co-adsorbant and device B: with co-adsorbant.

Dye	Device	Co-adsorbent	Electrolyte	TiO_2 [μm]	J_{SC} [mA cm^{-2}]	V_{OC} [V]	*FF*	η [%]
BTC-2	B	GBA (1:1)	Z984	7 + 5	16.1	0.75	0.74	9.1
	A		Z946	7 + 5	14.8	0.71	0.72	7.6
	B	GBA (1:1)	Z946	7 + 5	15.1	0.74	0.74	8.3
	B	GBA (1:1)	Z946	3	10.5	0.75	0.71	5.7
	B	GBA (1:1)	Z946	5	12.7	0.75	0.73	7.0
Z-907	A		Z946	7 + 5	14.8	0.70	0.71	7.5
	B	GBA (1:1)	Z946	3	8.9	0.81	0.74	5.4
	B	GBA (1:1)	Z946	5	11.1	0.80	0.74	6.6

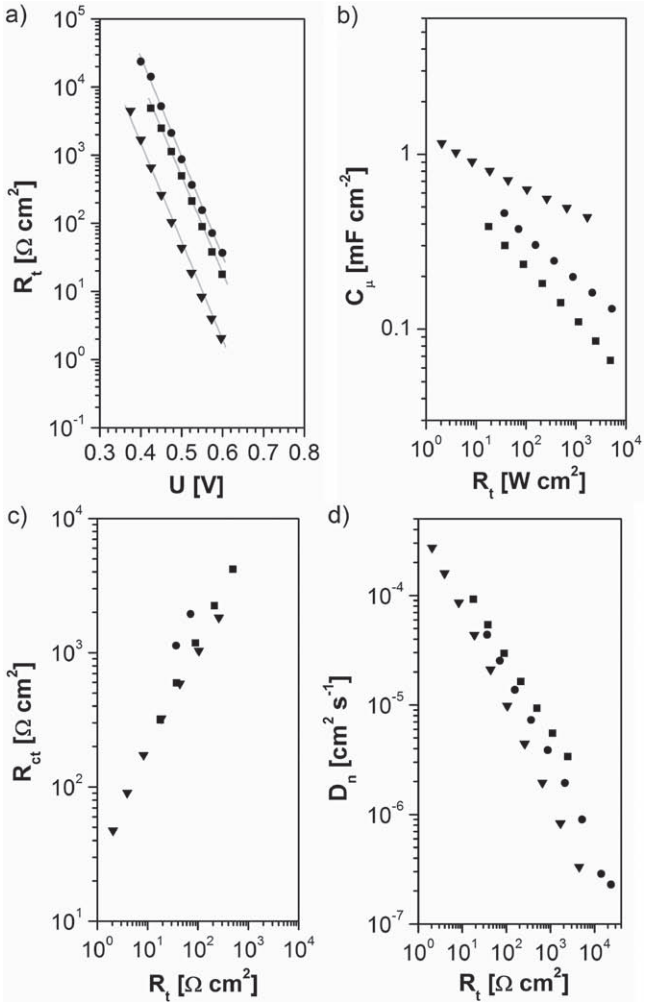

Figure 7. Derived equivalent circuit components obtained from impedance measurements under dark conditions at 20 °C as a function of electron transfer resistance for three different devices sensitized with ■: **BTC-2,** the fresh device A and ●,▼: **BTC-2**/GBA, the fresh device B and aged device B. a) Electron transport resistance R_t of the TiO_2 film, b) chemical capacitance (C_μ), c) recombination resistance (R_{ct}), and d) electron diffusion coefficients (D_n).

Figure 8a shows the charge density versus voltage plot for the fresh and aged device under full sunlight soaking at 60°C (device B). The photovoltage of the DSC is determined by the ratio of the values of free electron concentration in the TiO_2 film in the dark and under illumination.[4,13] The leftward shift (about 40 mV at the extracted charge density of 1×10^{18} cm^{-3}) in the charge density curve (the aged sample) can be interpreted as a downward movement (approximately a factor of 4.8) of the TiO_2 energy levels relative to the electrolyte. The lower band edge potential creates a larger driving force for the electron injection from the sensitizer; thus, a larger photocurrent was obtained in the aged sample as illustrated by the photovoltaic characteristics. Figure 8b shows the electron lifetimes for the fresh and aged cells plotted versus charge density. At an indicated charge density (1×10^{18} cm^{-3} for instance), the electron lifetime for the fresh device is about 1.7 times larger than for the aged one (0.1 ms vs 0.06 ms).

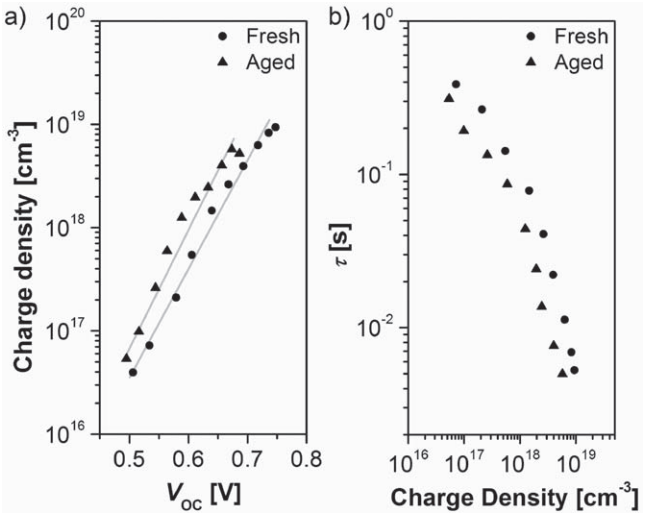

Figure 8. Transient photovoltage decay measurements of the fresh and aged devices with **BTC-2** and GBA (1:1 molar ratio): the effect of light soaking on the relationship a) between the photoinduced charge density and open circuit voltage and b) between the recombination lifetime and the photoinduced charge density.

In addition to liquid electrolytes solid-state (ss) devices with **BTC-2** and **Z-907** sensitizers using GBA as a co-adsorbent were prepared. In ss-devices the sensitizer **BTC-2** with 2,2′,7,7′-tetrakis-(*N*,*N*-di-*p*-methoxyphenylamine)-9,9′-spirobifluorene (spiro-MeOTAD) as hole transport material gave superior photovoltaic performance compared to **Z-907** using ultrathin mesoporous TiO_2 films (2 μm). The device with **BTC-2**/GBA and a 50-nm-particle TiO_2 film (2 μm) showed a J_{SC} of 7.5 mA cm^{-2}, a V_{OC} of 0.80 V, and a *FF* of 0.60, resulting in a η value of 3.6%. Under similar conditions a device based on **Z-907**/GBA gave J_{SC}, V_{OC}, *FF*, and η values of 6.0 mA cm^{-2}, 0.82 V, 0.60, and 3.1% at full sun light intensity. The advantage of the high molar extinction coefficient of the **BTC-2** dye is reflected in an increased J_{SC} value by approximately 25% compared to **Z-907** dye.

3. Conclusion

In summary, we have successfully developed a new heteroleptic ruthenium sensitizer **BTC-2** in which the anchoring carboxylic acid groups are attached to the thiophene units. The attachment of anchoring groups to the thiophene units lowered the LUMO energy level of the sensitizer. Extending the π-conjugation of the anchoring ligand increased the device performance in thin films as a result of the increased molar absoptivity and enhanced spectral response in the red wavelength region. Using 3-μm-thin mesoporous TiO_2 films, the device with **BTC-2** sensitizer achieved a higher solar-to-electricity conversion efficiency of 5.7% compared to 5.4% for **Z-907** using low-volatile electrolyte and GBA as co-absorbent. Thicker films that employed a light scattering double layer structure showed 8.3% efficiency for sensitizer **BTC-2** in combination with a low-volatile electrolyte that showed excellent stability measured under light-soaking at 60 °C. Electrochemical impedance spectroscopy

and transient photovoltage decay measurements revealed that the electron lifetime was reduced after long-term light soaking and the conduction band level of TiO_2 film was shifted downward. Furthermore, **BTC-2**-sensitized ss-devices showed a 16% increase in cell efficiency compared to **Z907**-sensitized cells, which is attributed to the increase in light harvesting efficiency and evidently improved net charge injection efficiency (J_{SC}). We believe that this work will contribute to the development of new anchoring ligands capable of enhancing the performance of Ru-based DSSCs.

4. Experimental Section

Ru(5,5′-(2,2′-bipyridine-4,4′-diyl)dithiophene-2-carboxylic acid)(4,4′-dinonyl-2,2′-bipyridine)(NCS)$_2$ Sodium Salt (BTC-2): $RuCl_2(p\text{-cymene})_2$ (112.4 mg, 0.184 mmol) and 4,4′-dinonyl-2,2′-bipyridine (150 mg, 0.367 mmol) were taken in a Schlenk tube and dissolved in dry DMF (30 mL). The reaction mixture was heated to 60°C under argon for 4 h with constant stirring. Subsequently, ligand **1** (150 mg, 0.367 mmol) was added to this reaction flask and the reaction mixture was heated in the dark at 140°C for 4 h. Finally, an excess of NH_4NCS (837 mg, 11.0 mmol) was added to the reaction mixture and the heating continued for another 4 h. The reaction mixture was cooled to room temperature and the solvent was removed by using a rotary evaporator under vacuum. Water was added to the flask and the insoluble solid was collected on a sintered glass crucible by suction filtration. The solid was washed with distilled water and diethyl ether and then dried under vacuum. The crude complex was dissolved in methanolic sodium hydroxide solution and purified on a Sephadex LH-20 column with methanol as the eluent. The collected main band was then slowly titrated with an acidic methanol solution (HNO_3) to pH 4.8 to isolate **BTC-2** complex. The precipitated dye was collected on a sintered glass crucible by suction filtration and dried. ^{1}H NMR (400 MHz, d_4-MeOH, δ): 0.8 (t, 3H), 0.85 (t, 3H), 1.1-1.5 (m, 24H), 1.57 (m, 2H), 1.82 (m, 2H), 2.65 (t, 2H), 2.91 (t, 2H), 7.12 (dd, J = 5.76, 0.93 Hz, 1H), 7.48 (d, J = 5.73 Hz, 1H), 7.54 (d, J = 2.20 Hz, 1H), 7.76 (d, J = 3.55 Hz, 1H), 7.83 (dd, J = 5.61, 0.96 Hz, 1H), 7.88 (d, J = 3.53 Hz, 1H), 8.03 (d, J = 3.84 Hz, 1H), 8.24 (d, J = 3.90 Hz, 1H), 8.27 (dd, J = 5.91, 1.71 Hz, 1H), 8.54 (s, 1H), 8.69 (s, 1H), 9.03 (s, 1H), 9.09 (d, J = 5.76 Hz, 1H), 9.16 (s, 1H), 9.26 (d, J = 5.91 Hz, 1H). Elemental Analysis for $C_{50}H_{55}N_6NaO_4RuS_4{\cdot}2H_2O$ calculated. C, 54.98; H, 5.44; N, 7.69%, found. C, 54.75; H, 5.45; N, 7.47%.

Device Fabrication: Screen-printed layers of TiO_2 particles were employed as photoelectrodes in this study. A 3 to 11 µm thick transparent film of 20-nm TiO_2 particles was printed on the fluorine doped SnO_2 (FTO) conducting glass electrode (NSG, 10 Ω cm^{-2}) for use as transparent films. For the double layer film, a 7 µm transparent film was first printed on FTO glass and subsequently coated with a 5-µm-thick second layer of 400 nm light-scattering anatase particles (CCIC, Japan). The porosity was determined from Brunauer–Emmett–Teller (BET) surface area measurements to be 68% for the 20-nm TiO_2 transparent layer and 42% for the 400-nm TiO_2 scatting layer. The detailed methods for TiO_2 film preparation, device fabrication, and the photocurrent–voltage measurements can be found in an earlier report.[14] After sintering at 500 °C and cooling to 80 °C, the sintered TiO_2 electrodes were sensitized by dipping for 16 h into the dye solution (300 µM) in 10% DMSO and acetonitrile and *tert*-butyl alcohol (volume ratio 1:1) mixture, with 300 µM GBA as a co-adsorbent. For the high-performance device, an acetonitrile-based electrolyte Z984 (0.6 M 1,3-dimethylimidazolium iodide (DMII), 0.05 M LiI, 0.03 M I_2, 0.5 M *tert*-butylpyridine, and 0.1 M guanidinium thiocyanate (GNCS) in the mixed solvent of acetonitrile and valeronitrile (v/v, 85/15)) was used. For the solid-state devices, a compact TiO_2 layer was first deposited onto the FTO substrate by spray pyrolysis, then 50-nm TiO_2 particles were deposited by doctor-blading to obtain a 2-µm-thick mesoporous film. After sintering the TiO_2 layers at 500 °C, the film was cooled to room temperature and immersed overnight in 0.02 M aqueous $TiCl_4$. The film was then rinsed with deionized water, annealed in air at 450 °C for 20 min and cooled to 80 °C before immersing it in the above mentioned dye solution for sensitization. The hole transporting material solution containing 0.17 M spiro-MeOTAD, 0.11 mM *tert*-butylpyridine, and 0.21 mM $LiN(CF_3SO_2)_2$ in chlorobenzene was used. The solution was deposited onto the dye-coated TiO_2 film, leaving it to penetrate into the pores of the TiO_2layer for 1 min prior to spin coating. Finally, a 50-nm-thick gold contact was deposited onto the organic semiconductor to close the cell.

Physicochemical and Photovoltaic Performance Measurements: NMR spectra were recorded on an Bruker Avance 400 spectrometer (^{1}H NMR: 400 MHz) at 25 °C. Chemical shift values (δ) are expressed in parts per million using residual solvent protons (DMSO-d_6: ^{1}H δ = 2.5 ppm and ^{13}C δ = 39.4 ppm) as an internal standard. Melting points were determined using a BuchiB-545 apparatus. Elemental analyses were carried out on a Heraeus CHN-O-S Rapid-F002 analysis system. Optical measurements were carried out in 1-cm cuvettes with Merck (Germany) spectroscopic grade solvents. Absorption spectra recorded on a Perkin Elmer Lambda 19 spectrometer and fluorescence spectra were recorded on a Perkin Elmer LS 55 spectrometer. The emission spectra are fully corrected for the photodetector response. Cyclic voltammetry experiments were performed with a computer-controlled Autolab PGSTAT30 potentiostat in a three-electrode single-compartment cell with a platinum working electrode, a platinum wire counter electrode, and an Ag/AgCl reference electrode. All potentials were internally referenced to the Fc/Fc$^+$ couple. The photovoltaic performance of cells, as well as the device stability, was measured using the methods reported in the literature.[4l]

Transient Photoelectrical Measurements: In the transient photovoltage decay experiments, different steady-state lights were supplied with a homemade white-light-emitting diode array by tuning the driving voltage and a red-light-emitting diode array controlled with a fast solid-state switch to generate a perturbation pulse with a width of 50 ms. The pulsed red- and steady-state white-lights were both incident on the photoanode side of the testing cell. The pulsed red lights were carefully controlled by the driving potential of the red diode array to keep the modulated photovoltage below 10 mV. We used red light as a probe to generate a photovoltage perturbation near the V_{OC} of the cell under the white light and measured the voltage decay process thereafter. Normally, the decay closely follows a monoexponential form, thus the recombination rate constant can be extracted from the slope of the semilogarithmic plot.

Electrochemical impedance spectroscopy (EIS) measurements were performed with an Autolab Frequency Analyzer setup, consisting of an Autolab PGSTAT 30 (Eco Chemie B.V., Utrecht, The Netherlands) for the production of small amplitude harmonic voltages and a frequency response analyzer module.[10]

Acknowledgements

A.M. and P.B thank the German Ministry of Education and Research (BMBF) in the frame of project OPEG 2010 and N.P, M.W, S. M, S.M.Z and M.G thank the Swiss National Science Foundation for the financial support.

Received: September 6, 2010
Published online: January 20, 2011

[1] a) B. O'Regan, M. Grätzel, *Nature* **1991**, *353*, 737; b) M. Grätzel, *Nature* **2001**, *414*, 338; c) A. Hagfeldt, M. Grätzel, *Acc. Chem. Res.* **2000**, *33*, 269.

[2] a) M. K. Nazeeruddin, A. Kay, L. Rodicio, R. Humpbry-Baker, E. Miiller, P. Liska, N. Vlachopoulos, M. Grätzel, *J. Am. Chem. Soc.* **1993**, *115*, 6382; b) M. K. Nazeeruddin, F. De Angelis, S. Fantacci, A. Selloni, G. Viscardi, P. Liska, M. Grätzel, *J. Am. Chem. Soc.* **2005**, *127*, 16835.

[3] a) D. Kuang, S. Ito, B.Wenger, C. Klein, J.-E. Moser, R. Humphry-Baker, S. M. Zakeerudddin, M. Grätzel, *J. Am. Chem. Soc.* **2006**, *128*, 4146; b) D. Kuang, C. Klein, H. J. Snaith, J. E. Moser,

R. Humphry-Baker, P. Comte, S. M. Zakeeruddin, M. Grätzel, *Nano Lett.* **2006**, *6*, 769; c) P. Wang, C. Klein, R. Humphry-Baker, S. M. Zakeeruddin, M. Grätzel, *J. Am. Chem. Soc.* **2005**, *127*, 808; d) P. Wang, C. Klein, R. Humphry-Baker, S. M. Zakeeruddin, M. Grätzel, *Appl. Phys. Lett.* **2005**, *86*, 123508; e) J. M. Kroon, N. J. Bakker, H. J. P. Smit, K. R. Thampi, P. Wang, S. M. Zakeeruddin, M. Grätzel, A. Hinsch, S. Hore, U. Wüfel, R. Sastrawan, J. R. Durrant, E. Palomares, H. Petterson, T. Gruszecki, J. Walter, K. Skupien, G. E. Tulloch, *Prog. Photovoltaics* **2007**, *15*, 1; f) D. Kuang, C. Klein, S. Ito, J. E. Moser, R. Humphry-Baker, N. Evan, F. Duriaux, S. M. Zakeeruddin, M. Grätzel, *Adv. Mater.* **2007**, *19*, 1133; g) S.-R. Jang, C. Lee, H. Choi, J. Ko, J. Lee, R. Vittal, K. J. Kim, *Chem. Mater.* **2006**, *18*, 5604; h) J.-J. Lagref, M. K. Nazeeruddin, M. Grätzel, *Synth. Met.* **2003**, *138*, 333; i) C. Klein, M. K. Nazeeruddin, P. Liska, D. Di Censo, N. Hirata, E. Palomares, J. R. Durrant, M. Grätzel, *Inorg. Chem.* **2005**, *44*, 178; j) S.-R. Jang, J.-H. Yum, C. Klein, K.-J. Kim, P. Wagner, D. Officer, M. Grätzel, M. K. Nazeeruddin, *J. Phys. Chem. C* **2009**, *113*, 1998; k) P. Wang, S. M. Zakeeruddin, J. E. Moser, R. Humphry-Baker, P. Comte, V. Aranyos, A. Hagfeldt, M. K. Nazeeruddin, M. Grätzel, *Adv. Mater.* **2004**, *16*, 1806.

[4] a) C. Y. Chen, S. J. Wu, C. G. Wu, J. G. Chen, K. C. Ho, *Angew. Chem.* **2006**, *118*, 5954; *Angew. Chem. Int. Ed.* **2006**, *45*, 5822; b) C. Y. Chen, S. J. Wu, J. Y. Li, C. G. Wu, J. G. Chen, K. C. Ho, *Adv. Mater.* **2007**, *9*, 3888; c) F. Gao, Y. Wang, J. Zhang, D. Shi, M. Wang, R. Humphry- Baker, P. Wang, S. M. Zakeeruddin, M. Grätzel, *Chem. Commun.* **2008**, 2635; d) F. Gao, Y.Wang, D. Shi, J. Zhang, M. Wang, X. Jing, R. Humphry-Baker, P. Wang, S. M. Zakeeruddin, M. Grätzel, *J. Am. Chem. Soc.* **2008**, *130*, 10720; e) D. Shi, N. Pootrakulchote, R. Li, J. Guo, Y. Wang, S. M. Zakeeruddin, M. Grätzel, P. Wang, *J. Phys. Chem. C* **2008**, *112*, 17046; f) C. Y. Chen, J. G. Chen, S. J. Wu, J. Y. Li, C. G. Wu, K. C. Ho, *Angew. Chem.* **2008**, *120*, 7452; *Angew. Chem. Int. Ed.* **2008**, *47*, 7342; g) A. Abbotto, C. Barolo, L. Bellotto, F. De Angelis, M. Grätzel, N. Manfredi, C. Marinzi, S. Fantacci, J. H. Yum, M. K. Nazeeruddin, *Chem. Commun.* **2008**, 5318; h) H. Choi, C. Baik, S. Kim, M. S. Kang, X. Xu, H. S. Kang, S. O. Kang, J. Ko, M. K. Nazeeruddin, M. Grätzel, *New J. Chem.* **2008**, *32*, 2233; i) Y. Cao, Y. Bai, Q. Yu, Y. Cheng, S. Liu, D. Shi, F. Gao, P. Wang, *J. Phys. Chem. C* **2009**, *113*, 6290; j) Q. Yu, S. Liu, M. Zhang, N. Cai, Y. Wang, P. Wang, *J. Phys. Chem. C* **2009**, *113*, 14559; k) F. Sauvage, M. K. R. Fischer, A. Mishra, S. M. Zakeeruddin, M. K. Nazeeruddin, P. Bäuerle, M. Grätzel, *ChemSusChem* **2009**, *2*, 761; l) C. Chen M. Wang, J. Li, N. Pootrakulchote, C. Alibabaei, J. Decoppet, J. Tsai, C. Grätzel, C. Wu, S. Zakeeruddin, M. Grätzel, *ACS Nano* **2009**, *3*, 3103.

[5] A. Mishra, N. Pootrakulchote, M. K. R. Fischer, C. Klein, M. K. Nazeeruddin, S. M. Zakeeruddin, P.Bäuerle, M. Grätzel, *Chem. Commun.* **2009**, 7146.

[6] Q. Wang, Z. Zhang, S. M. Zakeeruddin, M. Graetzel, *J. Phys. Chem C*, **2008**, *212*, 7084.

[7] J. Bisquert, V. Vikhrenko, *J. Phys. Chem. B* **2004**, *109*, 2313.

[8] J. Bisquert, D. Cahen, G. Hodes, S. Rühle, A. Zaban, *J. Phys. Chem. B* **2004**, *108*, 8106.

[9] M. Wang, P. Chen, R. Humphry-Baker, S. Zakeeruddin, M. Grätzel, *ChemPhysChem* **2009**, *10*, 290.

[10] M. Wang, X. Li, H. Lin, P. Pechy, S. M. Zakeeruddin, M. Grätzel, *Dalton Trans.* **2009**, *45*, 10015.

[11] J. Bisquert, *Phys. Chem. Chem. Phys.* **2008**, *10*, 49.

[12] J. Bisquert, *J. Phys. Chem B.* **2002**, *106*, 325.

[13] L. Peter, *Acc. Chem. Res.* **2009**, *42*, 1839.

[14] P. Wang, S. M. Zakeeruddin, P. Comte, R. Charvet, R. Humphry-Baker, M. Grätzel, *J. Phys. Chem. B* **2003**, *107*, 14336.